FULL PAPER

Textronics

ADVANCED
FUNCTIONAL
MATERIALS

www.afm-journal.d

Multifunctional Smart Textronics with Blow-Spun Nonwoven Fabrics

Dong Hae Ho, Siuk Cheon, Panuk Hong, Jong Hwan Park, Ji Won Suk, Do Hwan Kim, Joong Tark Han, and Jeong Ho Cho*

Here, the fabrication of nonwoven fabric by blow spinning and its application to smart textronics are demonstrated. The blow-spinning system is composed of two parallel concentric fluid streams: i) a polymer dissolved in a volatile solvent and ii) compressed air flowing around the polymer solution. During the jetting process with pressurized air, the solvent evaporates, which results in the deposition of nanofibers in the direction of gas flow. Poly(vinylidene fluoride-co-hexafluoropropylene) (PVdF-HFP) dissolved in acetone is blow-spun onto target substrate. Conductive nonwoven fabric is also fabricated from a blend of single-walled carbon nanotubes (SWCNTs) and PVdF-HFP. An all-fabric capacitive strain sensor is fabricated by vertically stacking the PVDF-HFP dielectric fabric and the SWCNT/PVdF-HFP conductive fabric. The resulting sensor shows a high gauge factor of over 130 and excellent mechanical durability. The hierarchical morphology of nanofibers enables the development of superhydrophobic fabric and their electrical and thermal conductivities facilitate the application to a wearable heater and a flexible heat-dissipation sheet, respectively. Finally, the conductive nonwoven fabric is successfully applied to the detection of various biosignals. The demonstrated facile and cost-effective fabrication of nonwoven fabric by the blow-spinning technique provides numerous possibilities for further development of technologies ranging from wearable electronics to textronics.

1. Introduction

The dramatic growth of the Internet of Things (IoT) industry is proof that human life is connected to information more than ever. Numerous technologies—ranging from mobile phones to wearable electronics—have been proposed for achieving a seamless connection between humans and information; all the devices used in daily life offer sufficient functionality for IoT. Among such technologies, wearable electronics has attracted attention in many industries because of the unique advantages offered by such devices, such as their ability to enable seamless connection between humans and information, applicability to personal healthcare monitoring systems, and compatibility with smart textiles.[1] For commercializing wearable electronics, companies are utilizing conventional rigid electronics in combination with conductive woven yarn. However, rigid electronics have the limitation of poor flexibility. To overcome this limitation, many research groups have been studying flexible smart textronics. Specifically, the use of smart textronics, in which woven or nonwoven fabric is employed to fabricate the complete range of electronic devices, is one of the most prominent ways to overcome the flexibility problem.[2] In addition to this research trend, the use of nanosized materials such as nanoparticles, carbon nanotubes (CNTs), and graphene has attracted considerable attention since the early 2000s owing to the unique characteristics of these materials resulting from their small sizes.[2b,3] Researchers in the field of textronics also partook in such research in order to realize and apply textile-based gadgets and to further enhance their functionality. Several methods have been used to fabricate nonwoven nanofiber fabrics that are aimed at achieving seamless hybridization between nanosized materials and textronics, such as melt-blow spinning, melt spinning, electrospinning, and solution spinning.[3f,4]

The production process of nonwoven fabric is shorter and easier than that of woven fabric; this consequently reduces the

D. H. Ho, S. Cheon, P. Hong, Prof. J. W. Suk
SKKU Advanced Institute of Nanotechnology (SAINT)
Sungkyunkwan University
Suwon 440-746, Republic of Korea
Dr. J. H. Park, Dr. J. T. Han
Nano Hybrid Technology Research Center
Korea Electrotechnology Research Institute (KERI)
Changwon 642-120, Republic of Korea

Prof. D. H. Kim
Department of Chemical Engineering
Hanyang University
Seoul 04763, Republic of Korea
Prof. J. H. Cho
Department of Chemical and Biomolecular Engineering
Yonsei University
Seoul 03722, Republic of Korea
E-mail: jhcho94@yonsei.ac.kr

**ADVANCED
SCIENCE NEWS**

www.advancedsciencenews.com

**ADVANCED
FUNCTIONAL
MATERIALS**

www.afm-journal.de

total processing cost of the former. Furthermore, nonwoven fabric has been demonstrated to have a wide range of applications, e.g., in filters,[4c,g,5] construction materials,[6] automotive materials,[7] fashion design,[8] batteries,[9] furniture,[10] and packaging.[11] Electrospinning is one of the promising methods for the fabrication of nonwoven nanofibers using a wide variety of polymers. Electrospinning involves the use of electric force to draw charged threads of polymers in solution form or melt form, where the fiber diameters are on the order of several hundred nanometers.[4d] Electrospinning operates under high voltages requiring extra cautious for handling. Also, the target materials for electrospinning should be electrically grounded, which can be achieved from a limited number of objects. Due to the dragging force applied in the concentrated areas, the freedom in the design for the equipment is restricted. For the top-down electrospinning, the nonuniformity of the spinning solution in time or in position is a challenging issue that restricts its application to mass production. For the bottom-up electrospinning, on the other hand, the formation of unwanted droplets arising from instantaneous nonuniformity in the electric field at the nozzle exit is a challenging issue to be resolved from reliable production.[12]

In this paper, we present, for the first time, blow-spun nonwoven fabric developed for application to smart textronics. Blow spinning is a fiber production method for producing nonwoven fabric that does not require as high a voltage as does electrospinning and that can rapidly produce nanofibers by using compressed air.[13] Poly(vinylidene fluoride-*co*-hexafluoropropylene) (PVdF-HFP) dissolved in acetone was blow-spun onto various target substrates. Both the concentration of the polymer solution and the air pressure were precisely adjusted to control the fibrous morphology and mechanical properties of the fabric. Conductive nonwoven fabric was fabricated through blow spinning of PVdF-HFP blended with conductive single-walled CNTs (SWCNTs). The blow-spun nonwoven fabric was successfully applied to various smart textronics: a capacitive strain sensor, superhydrophobic fabric, a wearable heater, a flexible heat-dissipation sheet, and biosignal (electromyogram (EMG), electrocardiogram (ECG), electroencephalogram (EEG), and electrodermal activity (EDA)) detection systems. The application of nonwoven fabrics as proposed in this work provides a novel and facile route to the realization of low-cost, wearable textronics.

2. Results and Discussion

Figure 1a shows a photographic image of the setup of the custom-made solution blow spinning equipment. The equipment consists of two components: i) an air compressor and ii) an airbrush. The air compressor is the compressed-gas source that contains pressurized air inside a metal tank and delivers air to the airbrush. The airbrush, which is a commercially available spray gun used for spray coating or painting, is composed of three parts: a nozzle, needle, and reservoir (Figure S1, Supporting Information). When the airbrush is triggered, the pressurized air supplied from the compressor passes through the outer nozzle. When the pressurized air passes through the outer nozzle, the polymer solution in the reservoir

is transferred to the front of the inner nozzle. The needle, controlled by the trigger, causes the movement of polymer solution toward the nozzle tip to blow out the nonwoven fabric. A convex droplet of the polymer solution is formed at the tip of the inner nozzle when there is no air flow through the outer nozzle. As air flow through the outer nozzle increases, the convex droplet is stretched by a high-pressure stream of compressed air flowing around the droplet through the outer nozzle, which consequently results in distortion of the droplet into a conical shape. Above the critical air pressure, the polymer solution jet erupts from the apical region of the cone and is accelerated to the target substrate.[13a,14] As these jets travel through the surrounding environment, they are stretched owing to a combination of the pressure gradient force and shearing at the solution–air interface, whereas the volatile solvent evaporates, leaving behind polymer nanofibers on the surface of the target substrate. The instant at which the nanofibers blew out from the nozzle tip of the airbrush was photographed using a high-speed camera (Figure 1b and Movie S1, Supporting Information). The captured image clearly shows the trajectory of the solution jet.

By this facile method, nonwoven fabric composed of nanofibers can be fabricated onto arbitrary substrates such as paper, plastic, and even human skin. Figure 1c shows blow spinning of nanofibers of PVdF-HFP dissolved in volatile acetone onto human skin. One should not deny that toxicity of acetone to human. However, because of its low boiling point, a major portion of the acetone would be vaporized while blow-spinning and only a marginal amount would make contact to the human skin. Furthermore, its toxicity is relatively smaller than other organic solvents (i.e., dimethylacetamide and triethyl phosphate) that can dissolve PVdF-HFP. PVdF-HFP is well known as one of the chemically and environmentally stable polymers. The blow-spun nanofiber mat on human skin could easily be peeled off from the skin surface, and the shape of the wearable fabric was also maintained (Figure 1d). One of the features of this blow-spun nonwoven fabric is that color printing can be performed on its surface. Figure 1e shows printing of patterns onto the fabric surface by the use of a commercial inkjet printer. Unlike the flat surface of PVdF-HFP (without a fibrous structure; see Figure S2, Supporting Information), nonwoven fabric composed of nanofibers contains fillable vacancies among the nanofibers, similar to paper made of cellulose pulp; this enables storage of color ink within the nanofiber network. Figure 1f shows a photographic image of blow-spun nonwoven fabric with inkjet-printed patterns. The patterns exhibit both sharp and clean edges and vivid colors in comparison to the flat surface of PVdF-HFP.

Both the concentration of the polymer solution and the pressure of compressed air are key parameters of the solution blow spinning process that govern the fibrous morphology and mechanical properties of the fabric. In this study, the physical dimensions of the PVdF-HFP nanofibers were deterministically controlled by varying both these parameters. Figure 1g shows a 3D chart of the fiber diameter as a function of air pressure and PVdF-HFP concentration. At low pressures, the stretching force was not sufficient for the formation of nanofibers. High air pressure led to an increase in the physical forces acting directly on the solution droplets being drawn, which resulted
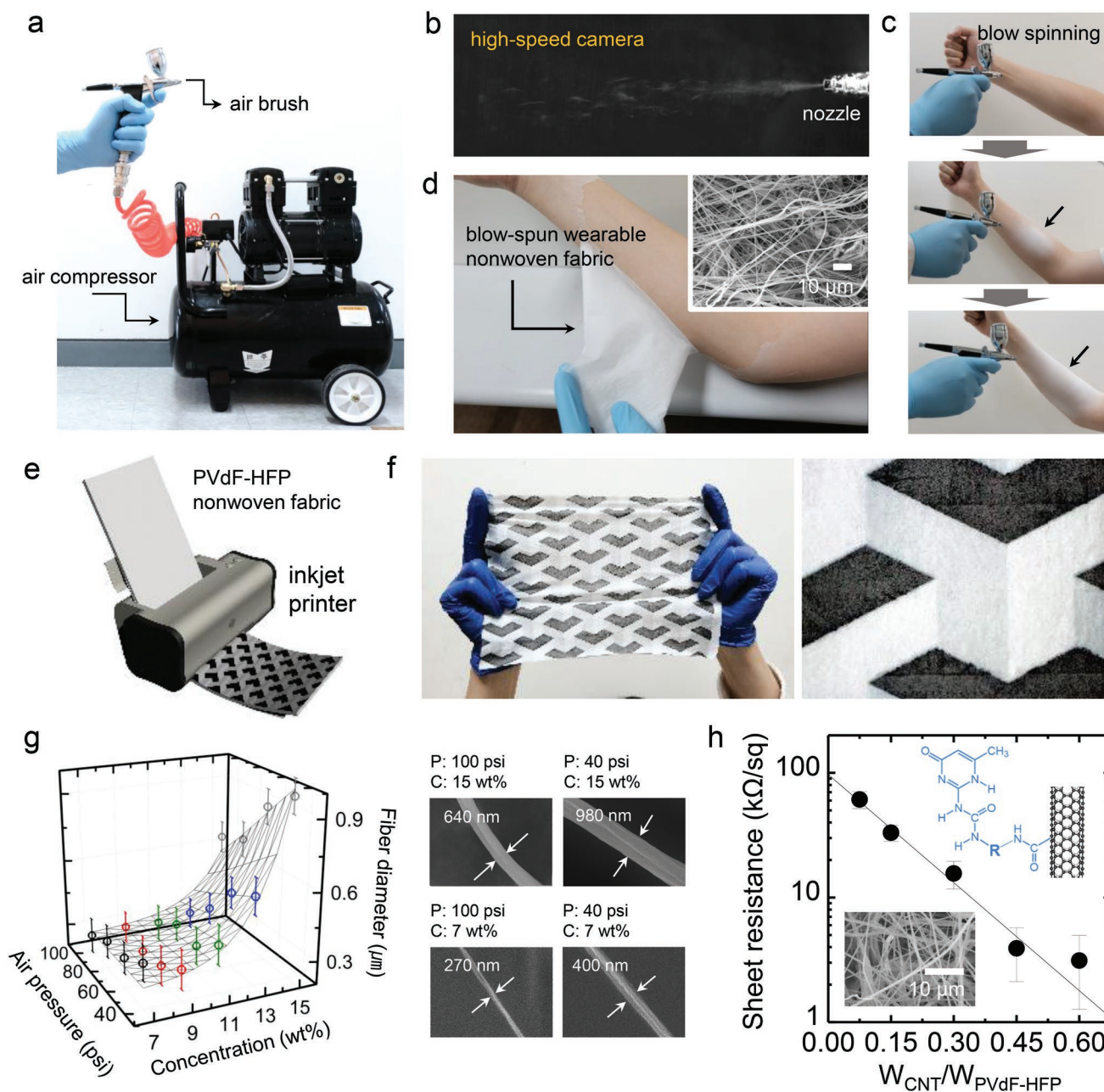
Figure 1. a) Photographic image of blow-spinning equipment composed of airbrush and air compressor. b) Photograph of nanofibers blowing out from nozzle tip of airbrush captured by high-speed camera. c) Chronological series of photographic images captured during blow spinning of PVdF-HFP nanofibers onto bare skin. d) Photographic image of nonwoven fabric being peeled off from bare skin. The inset shows an SEM image of the blow-spun nonwoven fabric. e) Schematic illustration of printing of pattern onto blow-spun nonwoven fabric by means of commercial inkjet printer. f) Inkjet-printed pattern on blow-spun nonwoven fabric. g) Pareto chart of fiber diameter as a function of air pressure and PVdF-HFP concentration. The right panel shows representative SEM images of nanofibers prepared under various spinning conditions. h) Plot of sheet resistance versus $W_{SWCNT}/W_{PVdF-HFP}$ ratio of blow-spun SWCNT/PVdF-HFP nonwoven fabric. The inset shows the chemical structure of the SWCNT functionalized with the 2-ureido-4[1H] pyrimidinone group and an SEM image of the SWCNT/PVdF-HFP nonwoven fabric.

in the formation of thin nanofibers. However, air pressures higher than 100 psi resulted in the formation of a large number of beads owing to turbulence, which were an undesirable by-product (Figure S3a, Supporting Information). At low air pressures below 40 psi, nanofibers with diameters larger than 900 nm were formed, but at such pressures, nozzle clogging occurred easily, and consequently, the productivity decreased

dramatically. The solution concentration was modified in the range of 7–15 wt% to obtain the nanofibers. This range was chosen because, similar to the case of air pressure, at concentrations lower than 7 wt%, fabric-containing beads were formed (Figure S3b, Supporting Information), whereas at concentrations higher than 15 wt%, jet instability and nozzle clogging occurred. With an increase in the solution concentration from

7 to 15 wt%, the fiber diameter increased from 270 to 980 nm. The right panel of Figure 1g shows representative scanning electron microscopy (SEM) images of the blow-spun nanofibers under various spinning conditions. For example, nanofibers with a diameter of 980 nm were obtained at a pressure of 40 psi and a solution concentration of 15 wt%, whereas nanofibers with a diameter of 270 nm were obtained at 100 psi and 7 wt%. Fracture strength point of the blow-spun fabric decreased from 1.74 to 0.68 MPa (Figure S4, Supporting Information) because the fabric with larger diameter nanofibers had lower junction density compared with smaller diameter case.

In order to fabricate conductive nonwoven fabric, PVdF-HFP was blended with SWCNTs. The SWCNTs were functionalized with supramolecular 2-ureido-4[1H]pyrimidinone (UPy) groups (upper inset of Figure 1h), which enabled their dispersion in acetone—the volatile solvent utilized to dissolve PVdF-HFP. This facilitated the formation of a percolation network of SWCNTs within the PVdF-HFP matrix. SWCNTs containing carboxylic acid or hydroxyl groups were reacted with 2(2-methyl-5-isocyanatobenzylaminocarbonylamino)-6-methyl-4[1H]-pyrimidinone in order to introduce UPy groups on their surfaces and edges. The blow-spun fabric prepared with a weight fraction ($W_{SWCNT}/W_{PVdF-HFP}$) of 0.1 was conductive because of the formation of the percolation network of the SWCNTs. As the $W_{SWCNT}/W_{PVdF-HFP}$ ratio increased from 0.1 to 0.6, the sheet resistance decreased from 61.2 to 3.1 kΩ sq^{-1} because of strengthening of the percolation effects. Much higher concentration of SWCNT above the percolation threshold of the network was required to form conductive pathways through the fabric. In addition, the conductive nonwoven fabric exhibited the long-term environmental stability as shown in Figure S5 in the Supporting Information. The lower inset of Figure 1h shows a SEM image of PVdF-HFP with $W_{SWCNT}/W_{PVdF-HFP}$ of 0.1, whose morphology is similar to that of pristine PVdF-HFP nanofibers. The resulting conductive nonwoven fabric was successfully applied to a variety of textronics.

First, the blow-spun fabrics were utilized as a capacitive strain sensor. **Figure 2**a shows the fabrication procedure of a capacitive strain sensor based on vertically stacked PVdF-HFP dielectric fabric and the SWCNT/PVdF-HFP conductive fabric. The PVdF-HFP nanofibers were blow-spun onto a plastic film as a wearable substrate. A shadow mask was placed on the PVdF-HFP fabric, and then, acetone solution with a $W_{SWCNT}/W_{PVdF-HFP}$ ratio of 0.45 was blow-spun to pattern the SWCNT/PVdF-HFP conductive fabric as the bottom electrodes. PVdF-HFP was blow-spun through the shadow mask to form the strain-sensitive dielectric layer. Finally, the SWCNT/PVdF-HFP fabric acting as the conductive top electrodes was patterned onto the PVdF-HFP fabric via blow spinning. A nominal strain (δ) was applied to the strain sensor by using a custom-made bending machine (inset of Figure 2b). The capacitance (C) value of the sensor increased from 2.7 to 3.7 pF with an increase in δ from 0% to 0.3%. Furthermore, the signal of the sensor exhibited negligible hysteresis during forward and reverse sweeps. Figure 2c shows the normalized capacitance ($\Delta C/C_0$) of the sensor, where C_0 is the initial capacitance in the absence of external strain and ΔC is equal to $C − C_0$. The gauge factor (GF), the slope of the plot in Figure 2c, of the sensor was found to be around 134. This remarkably high GF was strongly related

to the fibrous morphologies of both the conductive fabric and the dielectric fabric. The measured C of the strain sensor was expressed as $\varepsilon A/d$, where d is the distance between the two electrodes, A is the area of electrode, and ε is the permittivity. When the nominal strain was applied to the sensor, the contact area at numerous junctions between the electrode and the dielectric nanofibers (A) changed sensitively, which significantly increased the capacitance of the sensor. Along with the increase in A, the distance between the two electrodes (d) decreased significantly by sensitive deformation of the porous fibrous structure. Synergetic effects of i) an increased contact area between the dielectric layer and the electrode layer and ii) the reduced distance between the two electrodes may have contributed to the high GF of our strain sensor. Further, δ of up to 5% was applied using acrylic rods with various radii to check the sensing range of the strain sensor (Figure S6, Supporting Information). It is noteworthy that the sensor exhibited a superlinear response to δ over a wide range of δ.

Next, a real-time strain test was performed, as shown in Figure 2d. In this test, strain was applied in 10 steps, from 0.04% to 0.15%, and capacitance was measured as a function of time. The discrete signal levels at each strain were observed; signals at increasing and decreasing steps were found to be at the same level. A durability test was also performed, as shown in Figure 2e, wherein a strain of 0.1% was applied repetitively for 1000 cycles. Magnified plots in the time periods of 5–10 s and 1955–1960 s showed consistent values at the start and end of the durability test. In Figure 2f, a distinguishable signal could be observed both in the absence of strain and under application of an extremely low strain of 0.03%. The minimum detectable strain was found to be as low as 0.03%. In addition, the rise and fall times were found to be less than 100 ms. A 4 × 4 strain sensor array was successfully fabricated for mapping the spatial pattern of the strains applied to the matrix. Figure 2g shows the circuit design of a passive-matrix capacitive strain sensor array with top and bottom electrodes. A nominal strain was applied between two corners or two edges of the matrix (Figure 2h). The capacitance values of all pixels were then measured, and 2D grayscale color mapping of the strain distribution on the matrix was demonstrated (upper-right panel of Figure 2h). Here, white and black colors indicated the highest and lowest capacitances, respectively. The measured capacitances were simulated to generate a 3D gradient strain map with red and black colors, which yielded a configuration almost identical to the actual photographic image of the matrix.

Next, the blow-spun nonwoven fabrics were applied for various purposes, as demonstrated in **Figure 3**. First, the fabricated blow-spun fabric was employed as a superhydrophobic fabric. A spin-coated PVdF-HFP film showed a water contact angle of only 121°. Blow spinning significantly increased the water contact angle because of the multiscale hierarchical morphology of the fibers, as shown in Figure 3a. The surface wettability was systematically controlled by varying the solution concentration of PVdF-HFP. At a concentration of 5 wt%, a large number of popcorn-like beads that did not have a fibrous structure were formed in the fabric. The water contact angle at this concentration was measured to be around 140°. As the solution concentration increased from 5 to 9 wt%,
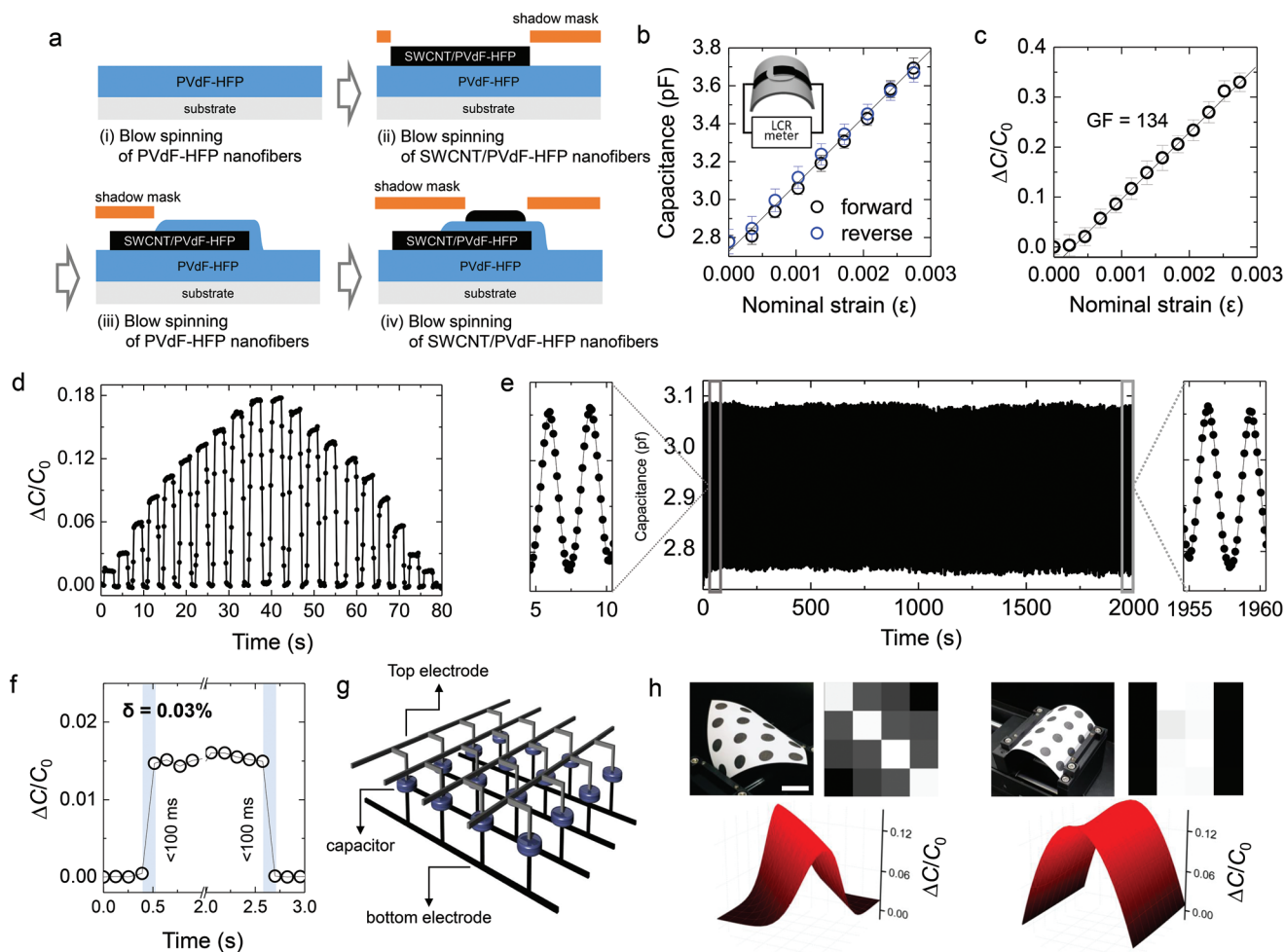
**ADVANCED
SCIENCE NEWS**

www.advancedsciencenews.com

**ADVANCED
FUNCTIONAL
MATERIALS**

www.afm-journal.de

Figure 2. a) Schematic of fabrication procedure of all-fabric-type capacitive strain sensor. b) Capacitance of strain sensor as a function of nominal strain. c) Plot of normalized capacitance of strain sensor ($\Delta C/C_0$) versus nominal strain. d) Real-time capacitance sensing of strain sensor under specific nominal strains (0.04%, 0.05%, 0.06%, 0.07%, 0.08%, 0.09%, 0.1%, 0.12%, 0.14%, and 0.15%). e) Stability test of strain sensor over 1000 cycles. f) Measurement of minimum detectable strain and response time of strain sensor. g) Schematic circuit diagram of passive-matrix strain sensor array. h) Test results of passive-matrix strain sensor array. The upper panel shows photographic images of the strain sensors under strains and corresponding 2D mapping of the strain distribution. The lower panel shows 3D mapping of the strain distribution (scale bar: 4 cm).

hierarchical structures containing beads and fibers developed significantly. These beads-on-string structures increased the water contact angle to up to 158°. At a solution concentration higher than 9 wt%, the number of beads decreased drastically, and a morphological transition occurred from the beads-on-string structure to the fibrous structure, which consequently decreased the water contact angle to 143°. The superhydrophobicity of our blow-spun nonwoven fabric was attributed to a combination of the low surface energy of PVdF-HFP and the hierarchical morphology of the fibrous structures formed by blow spinning. In particular, our fabric exhibited gecko-state superhydrophobicity, which is not only superhydrophobic but also strongly adhesive to water (Figure S7, Supporting Information). This high water-adhesive behavior arose from a large van der Waals force between the fibrous structures of the fabric and water.[15]

Second, the blow-spun conductive fabric was applied as a flexible electrothermal heater that converts electric power to heat. PVdF-HFP has excellent mechanical and thermal

stabilities, making it suitable for application to wearable heaters. Figure 3b shows the surface temperature of the fabric as a function of the input power. The conductive fabric (2 × 4 cm², thickness = ≈0.5 mm) with sheet resistance of around 50 kΩ sq⁻¹ was utilized. DC power was applied between two electrodes formed at the corner of the fabric, and then, the surface temperature of the fabric was monitored using a thermal imaging camera (inset of Figure 3b). As the input power increased to 0.8 W, the fabric temperature linearly increased to 66 °C because of Joule heating. A considerably sharp increase in the surface temperature was observed at input powers higher than 0.8 W. Even though the power efficiency of the developed heater was not high enough (≈60 K W⁻¹), its simple fabrication on any arbitrary surface and high mechanical and thermal stabilities are expected to prove useful in the fabrication of wearable heaters.

Third, the blow-spun conductive fabric (sheet resistance = ≈3 kΩ sq⁻¹) and dielectric fabric were separately applied as a flexible heat-dissipation sheet. Specifically, blow-spun fabrics with

**ADVANCED
SCIENCE NEWS**

www.advancedsciencenews.com

**ADVANCED
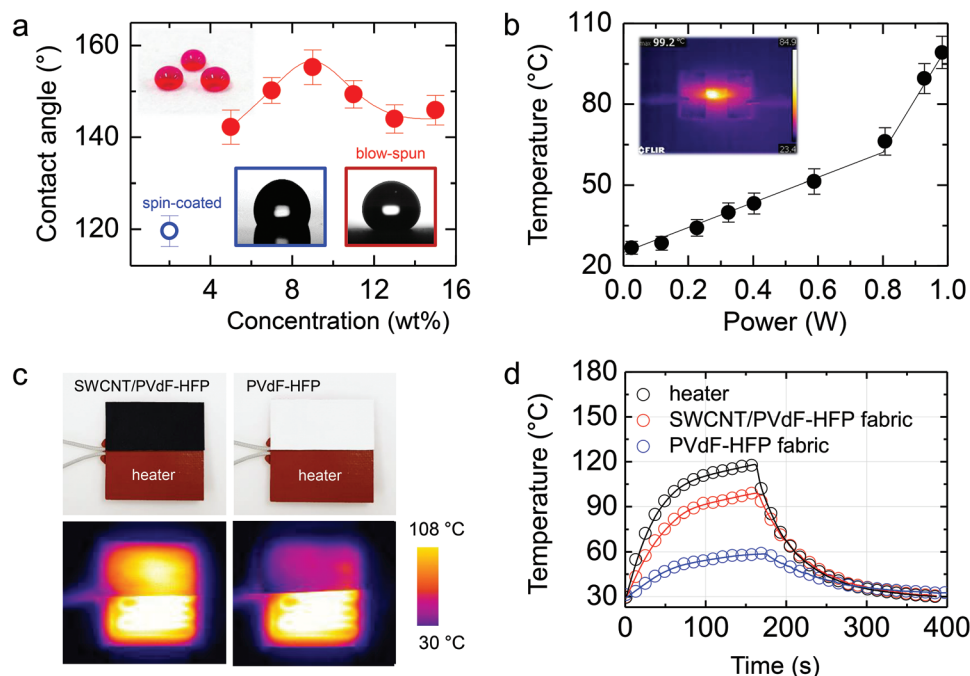FUNCTIONAL
MATERIALS**

www.afm-journal.de

Figure 3. a) Water contact angle of PVdF-HFP fabric prepared with various solution concentrations. The inset shows a photographic image of water droplets dropped on the fabric. b) Temperature of SWCNT/PVdF-HFP fabric heater as a function of applied power. The inset shows image captured by the thermal imaging camera. c) Photographic images of experimental setup for measuring heat dissipation properties (upper panel) and IR thermal images of SWCNT/PVdF-HFP fabric and PVdF-HFP fabric on heater captured at 160 s (lower panel). d) Surface temperatures of heater, SWCNT/PVdF-HFP fabric, and PVdF-HFP fabric as functions of time during heating and subsequent cooling.

a thickness of around 1 mm each were attached on top of a silicone heater, as shown in the upper panel of Figure 3c. The heater was heated with a power of 6.4 W for 160 s and then turned off. The surface temperatures of both the heater and the fabrics were monitored using a thermal imaging camera. The lower panel of Figure 3c shows the thermal images captured at 160 s. Figure 3d shows the surface temperatures of the heater and both the nonwoven fabrics as functions of time during heating and the subsequent cooling. When the heater was heated to 119 °C, the temperature of the PVdF-HFP dielectric fabric reached 58 °C. However, the temperature of the SWCNT/PVdF-HFP conductive fabric was around 100 °C because the SWCNTs acted as heat-conductive fillers. The mean free path of phonons inside PVdF-HFP was extremely short because of their scattering caused by the numerous defects present in PVdF-HFP; this led to the low thermal conductivity of the PVdF-HFP fabric. However, in the case of the SWCNT/PVdF-HFP composite fabric, the percolation network among the SWCNTs provided a pathway for phonon conduction; this resulted in lengthening of the mean free path of phonons (Figure S8, Supporting Information) and similar thermal conduction behavior with metallic copper.

Finally, the blow-spun SWCNT/PVdF-HFP conductive nonwoven fabric was successfully applied as biocompatible electrodes of biomedical devices. **Figure 4**a shows the BITalino biomedical kit used to measure four different biosignals (EMG, ECG, EEG, and EDA). The conductive fabric fabricated by blow spinning was cut into a circular shape for the purpose of pasting it onto the biosignal measurement patch. The measured signals were transferred to a remote device

using the Bluetooth module. First, the ECG was recorded for monitoring the heartbeat. Electrocardiography is the process of recording the electrical activity of the heart over a period by means of electrodes attached to human skin.[16] For ECG measurement, three patches of conductive fabric were attached, one each to the left arm, right arm, and left leg (Figure S9, Supporting Information). These electrodes detect minute electrical changes on the skin caused by electrophysiological pattern of depolarization and repolarization of the heart muscles during each heartbeat. ECG measurements are commonly performed in a cardiology test. During the ECG measurement, the subject performed three different activities: standing, running, and relaxing. As shown in Figure 4b, a heart rate of 75 bpm was observed when the subject was standing. During the running activity, the heartbeat rate increased to 150 bpm. When the subject took rest, i.e., relaxed, after running, the heartbeat rate decreased to 105 rpm. Second, the EMG was measured using the patch of the blow-spun conductive fabric. Electromyography is an electrodiagnostic medicine–based technique for evaluating and recording the electrical activity produced by skeletal muscles.[17] As shown in Figure 4c, two patches of the conductive fabric were attached to the flexor part of the wrist on the arm, and then, the output signal was measured during clenching of the subject's fist with maximum force. There was no output voltage when no force was applied, as seen in the light gray region. Application of force resulted in an output voltage of 1.5 mV, as seen in the dark gray region.

In the next step, the EDA of five subjects was measured. EDA is a property of the human body that causes continuous
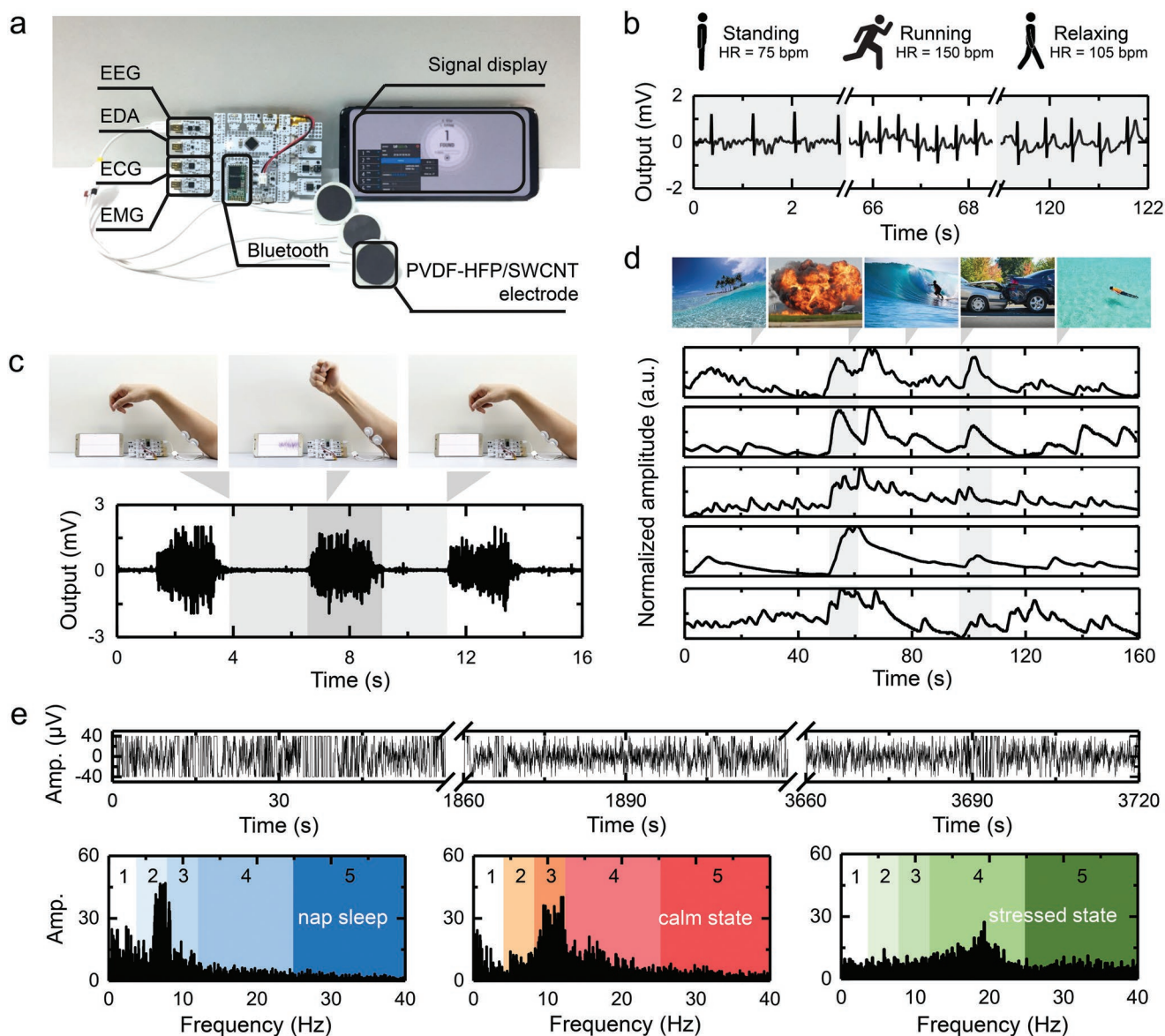
Figure 4. a) Photographic image of equipment used for biosignal measurements. The biosignals—EEG, EDA, ECG, and EMG—were measured using a biosensor kit and SWCNT/PVdF-HFP fabric electrodes. b) ECG measurement results obtained during three different activities: standing, running, and relaxing. c) EMG measurement results obtained when the subject's fist was clenched with maximum force and when the subject's arm was relaxed. The fabric electrodes were attached on the arm. d) Results of EDA tests of five different subjects. The upper panel shows the images constituting the video that was shown to the subjects. e) EEG measurement results (upper panel) and plot of amplitude versus frequency interpreted by FFT (lower panel). The subject was asked to perform three different activities: napping, being in a normal (calm) state, and solving math problems.

variation in the electrical characteristics of the skin. The resistance of skin varies with the state of sweat glands in the skin. Sweating is controlled by the sympathetic nervous system; skin conductance is an indication of psychological or physiological arousal. The sweat gland activity increases when the sympathetic branch of the autonomic nervous system is highly aroused, and this, in turn, increases the skin conductance. Therefore, skin conductance is a potential measure of emotional and sympathetic responses. For our EDA measurement, two patches of the conductive fabric were attached on the volar surface of the distal phalanges (Figure S9, Supporting Information). To measure the detectable difference between calm

and excited emotional states, a short video (70 s in length) that contained several images for triggering the desired arousal and valence signals was selected. The video, which contained two simulated trigger points, was simultaneously shown to the five subjects in the same location and each output signal was monitored during their viewing.[18] In Figure 4d, the two simulated trigger points are represented by the light gray region; here, the photographs in the upper panel are images selected from all images in the video. The magnitude and position of the signals were observed to differ from subject to subject. However, for all five subjects, stimulation was observed at identical points as intended.[19] Different signals were observed in

different regions depending on the subject given their diverse backgrounds.

Lastly, the EEG was measured by attaching three patches of the conductive fabric, one each at frontal pole 1, frontal 7, and the left earlobe (Figure 4e and Figure S9, Supporting Information). Electroencephalography is an electrophysiological monitoring method for recording the electrical activity of the brain. This method entails measurement of voltage fluctuations resulting from the flow of ionic current within the neurons of the brain. The collected brain wave data analyzed via fast Fourier transform (FFT) are shown in the lower panel of Figure 4e. The amplitude–frequency plot interpreted by FFT showed the peaks at each specific frequency; here, the peak position represents the behavior of the brain. Each brain wave signal was divided into five parts: i) delta wave (0–4 Hz), ii) theta wave (4–8 Hz), iii) alpha wave (8–12 Hz), iv) beta wave (12–40 Hz), and v) gamma wave (40 Hz or higher).[20] The brain waves were observed in a specific section depending on the physical and mental conditions of the subjects. The EEG electrodes were attached prior to the start of the measurement. Before the measurements, the impedance of the skin-electrode contact was confirmed to be lower than 10 kΩ at the sampling frequencies (Figure S10, Supporting Information). As shown in Figure 4e, the brain wave signal was measured for 1 h during various activities. The measurement was begun with the subject taking a nap in a comfortable position. The theta wave from 4 to 8 Hz was observed, which appeared during rapid-eye-movement sleep. After 30 min, the subject was woken up from the nap (red shaded area). The peak occurred in the beta region, which is typically observed when a human is in the nonattentional state. After 10 min, the subject was provided with a set of difficult math problems and asked to solve it within a certain time period. The peak mainly occurred in the beta region, as indicated by the green shaded area. High-frequency, low-amplitude beta waves are often observed for a human in an active, complex, anxious, and attentional psychological state.

3. Conclusion

In conclusion, we reported smart textronics applications based on blow-spun nonwoven fabrics. Conductive nonwoven fabric was fabricated by blow spinning of a blend of SWCNTs and PVdF-HFP dissolved in acetone. A capacitive strain sensor based on vertically stacked SWCNT/PVdF-HFP–SWCNT/PVdF-HFP–PVdF-HFP fabrics showed a high GF of 134, a minimum detectable strain of 0.03%, and excellent mechanical durability over 1000 cycles. The SWCNT/PVdF-HFP conductive nonwoven fabric was also successfully employed as a superhydrophobic fabric and applied to a wearable heater and a flexible heat-dissipation sheet. Finally, various types of biosignals (EMG, ECG, EEG, and EDA) were successfully detected using electrodes based on the SWCNT/PVdF-HFP conductive nonwoven fabric. The successful use of nonwoven fabrics prepared by the blow-spinning technique in various textronics applications as demonstrated in the present study is expected to usher in a new era of wearable electronics.

4. Experimental Section

Blow Spinning: Poly(vinylidene fluoride-*co*-hexafluoropropylene) (PVdF-HFP, Sigma-Aldrich, M_w = 400000) was dissolved in acetone at various concentrations and then stirred for 3 h at room temperature. The SWCNT (Nano Solution Inc.) had a diameter of 1.4–1.7 nm and a length of 5–20 μm. Separately, SWCNT functionalized with 2-ureido-4[1H]pyrimidinone groups were dispersed in acetone. Both solutions were mixed in various ratios and then placed in a sonication bath for 90 min. Five milliliters of the preprepared solution was loaded into the reservoir of an airbrush (FD-116A, Falcon). The airbrush nozzle was 0.2 mm in size. The airbrush was connected to an air compressor with a maximum pressure of 120 psi (ULTRA 340, AirFactory). The distance between nozzle and collector was 40–60 cm.

Characterization: The capacitive strain sensor was characterized using an Agilent E4980a LCR meter with a custom-made bending machine. A nominal strain was applied using a precision motor controller with an accuracy of 5 μm. The sheet resistance of the SWCNT/PVdF-HFP conductive nonwoven fabric was measured using RSP-50k. The i-SPEED 210 high-speed camera was used to observe the trajectory of the solution jet during blow spinning. An FLIR T420 thermal imaging camera was used to acquire IR thermal images and measure the surface temperature. The BITalino (r)evolution Board kit was used to measure the biological signals. The signals measured by the kit were wirelessly transferred to a remote device. The conductive nonwoven fabric was cut into a circular shape and attached on top of adhesive foam tape by means of a metal clip button to establish an electrical connection between the kit and the sensing electrode. The fabric electrodes were attached directly on bare skin.

Conflict of Interest

The authors declare no conflict of interest.

[1] a) J. McCann, D. Bryson, Textile Institute (Manchester England), *Smart Clothes and Wearable Technology*, CRC Press, Cambridge, Boca Raton, FL **2009**; b) S. P. Lee, G. Ha, D. E. Wright, Y. J. Ma,

**ADVANCED
Science News**

www.advancedsciencenews.com

**ADVANCED
FUNCTIONAL
MATERIALS**

www.afm-journal.de

E. Sen-Gupta, N. R. Haubrich, P. C. Branche, W. H. Li, G. L. Huppert, M. Johnson, H. B. Mutlu, K. Li, N. Sheth, J. A. Wright, Y. G. Huang, M. Mansour, J. A. Rogers, R. Ghaffari, *NPJ Digital Med.* **2018**, *1*, 2; c) J. Heikenfeld, A. Jajack, J. Rogers, P. Gutruf, L. Tian, T. Pan, R. Li, M. Khine, J. Kim, J. Wang, J. Kim, *Lab Chip* **2018**, *18*, 217; d) K. Dong, Y. C. Wang, J. N. Deng, Y. J. Dai, S. L. Zhang, H. Y. Zou, B. H. Gu, B. Z. Sun, Z. L. Wang, *ACS Nano* **2017**, *11*, 9490; e) Z. N. Bao, X. D. Chen, *Adv. Mater.* **2016**, *28*, 4177; f) Z. Ma, S. Li, H. T. Wang, W. Cheng, Y. Li, L. J. Pan, Y. Shi, *J. Mater. Chem. B* **2019**, *7*, 173.

[2] a) K. Cherenack, L. van Pieterson, *J. Appl. Phys.* **2012**, *112*, 091301; b) S. Coyle, Y. Z. Wu, K. T. Lau, D. De Rossi, G. Wallace, D. Diamond, *MRS Bull.* **2007**, *32*, 434; c) S. Jung, T. Ji, V. K. Varadan, *Smart Mater. Struct.* **2006**, *15*, 1872; d) M. Rothmaier, M. P. Luong, F. Clemens, *Sensors* **2008**, *8*, 4318; e) A. Schwarz, L. Van Langenhove, P. Guermonprez, D. Deguillemont, *Text. Prog.* **2010**, *42*, 99.

[3] a) I. S. Bayer, D. Fragouli, A. Attanasio, B. Sorce, G. Bertoni, R. Brescia, R. Di Corato, T. Pellegrino, M. Kalyva, S. Sabella, P. P. Pompa, R. Cingolani, A. Athanassiou, *ACS Appl. Mater. Interfaces* **2011**, *3*, 4024; b) Y. Cha, K. Nam, D. Kim, *Sensors* **2017**, *17*, 584; c) S. Cheon, H. Kang, H. Kim, Y. Son, J. Y. Lee, H. J. Shin, S. W. Kim, J. H. Cho, *Adv. Funct. Mater.* **2018**, *28*, 1703778; d) X. H. Guo, Y. Huang, C. Wu, L. D. Mao, Y. Wang, Z. C. Xie, C. X. Liu, Y. G. Zhang, *Smart Mater. Struct.* **2017**, *26*, 105036; e) S. Libertino, M. R. Plutino, G. Rosace, *AIP Conf. Proc.* **2018**, *1990*, 020016; f) A. K. Yetisen, H. Qu, A. Manbachi, H. Butt, M. R. Dokmeci, J. P. Hinestroza, M. Skorobogatiy, A. Khademhosseini, S. H. Yun, *ACS Nano* **2016**, *10*, 3042.

[4] a) N. Bhardwaj, S. C. Kundu, *Biotechnol. Adv.* **2010**, *28*, 325; b) T. Dias, *Electronic Textiles: Smart Fabrics and Wearable Technology*, Elsevier, Boston, MA **2015**; c) A. Greiner, J. H. Wendorff, *Angew. Chem., Int. Ed.* **2007**, *46*, 5670; d) Z. M. Huang, Y. Z. Zhang, M. Kotaki, S. Ramakrishna, *Compos. Sci. Technol.* **2003**, *63*, 2223; e) A. Schwarz, L. Van Langenhove, in *Multidisciplinary Know-How for Smart-Textiles Developers* (Ed: T. Kirstein), Woodhead Publishing, UK **2013**, p. 29; f) H. Yoshimoto, Y. M. Shin, H. Terai, J. P. Vacanti, *Biomaterials* **2003**, *24*, 2077; g) F. Dotti, A. Varesano, A. Montarsolo, A. Aluigi, C. Tonin, G. Mazzuchetti, *J. Ind. Text.* **2007**, *37*, 151; h) I. Karbownik, O. Rac, M. Fiedot, P. Suchorska-Woźniak, H. Teterycz, *Eur. Polym. J.* **2015**, *69*, 385; i) I. Karbownik, T. Rybicki, A. Karpinska, H. Teterycz, *Mater. Sci.-Pol.* **2016**, *34*, 564; j) A. Laforgue, M. F. Champagne, J. Dumas, L. Robitaille, *J. Eng. Fibers Fabr.* **2012**, *7*, 118; k) M. Latifi, P. Payvandy, M. Yousefzadeh-Chimeh, in *Technical Textile Yarns* (Eds: R. Alagirusamy, A. Das), Woodhead Publishing, UK **2010**, p. 298; l) S. Nair, E. Hsiao, S. H. Kim, *J. Mater. Chem.* **2008**, *18*, 5155; m) R. Nayak, I. L. Kyratzis, Y. B. Truong, R. Padhye, L. Arnold, G. Peeters, L. Nichols, M. O'Shea, *Adv. Mater. Res.* **2012**, *472–475*, 1294; n) R. Sinclair, *Textiles and Fashion: Materials, Design and Technology*, Elsevier, Boston, MA **2014**.

[5] a) Z. W. Ma, M. Kotaki, S. Ramakrishna, *J. Membr. Sci.* **2005**, *265*, 115; b) W. Sambaer, M. Zatloukal, D. Kimmer, *Chem. Eng.*

Sci. **2011**, *66*, 613; c) B. Tabti, M. R. Mekideche, M. C. Plopeanu, L. T. M. Dumitran, L. Herous, L. Dascalescu, *IEEE Trans. Ind. Appl.* **2010**, *46*, 634; d) B. Khalid, X. P. Bai, H. H. Wei, Y. Huang, H. Wu, Y. Cui, *Nano Lett.* **2017**, *17*, 1140.

[6] a) A. S. Herrmann, J. Nickel, U. Riedel, *Polym. Degrad. Stab.* **1998**, *59*, 251; b) R. Kozlowski, M. Malgorzata, M. Bozena, *Polym. Degrad. Stab.* **2011**, *96*, 396; c) S. Ramakrishna, K. Fujihara, W. E. Teo, T. Yong, Z. W. Ma, R. Ramaseshan, *Mater. Today* **2006**, *9*, 40.

[7] a) Y. Chen, O. Chiparus, L. Sun, I. Negulescu, D. V. Parikh, T. A. Calamari, *J. Ind. Text.* **2005**, *35*, 47; b) G. Thilagavathi, E. Pradeep, T. Kannaian, L. Sasikala, *J. Ind. Text.* **2010**, *39*, 267; c) X. Ye, R. Fangueiro, H. Hu, M. de Araujo, *J. Text. Inst.* **2007**, *98*, 337.

[8] a) K. Anderson, *Nonwovens Ind.* **2005**, *36*, 40; b) F. M. Ng, *Res. J. Text. Apparel* **2004**, *8*, 65; c) M. Wang, H. J. Jin, D. L. Kaplan, G. C. Rutledge, *Macromolecules* **2004**, *37*, 6856.

[9] a) T. H. Cho, M. Tanaka, H. Onishi, Y. Kondo, T. Nakamura, H. Yamazaki, S. Tanase, T. Sakai, *J. Power Sources* **2008**, *181*, 155; b) S. W. Choi, S. M. Jo, W. S. Lee, Y. R. Kim, *Adv. Mater.* **2003**, *15*, 2027; c) J. L. Hao, G. T. Lei, Z. H. Li, L. J. Wu, Q. Z. Xiao, L. Wang, *J. Membr. Sci.* **2013**, *428*, 11; d) Y. E. Miao, G. N. Zhu, H. Q. Hou, Y. Y. Xia, T. X. Liu, *J. Power Sources* **2013**, *226*, 82.

[10] a) T. A. Bullions, D. Hoffman, R. A. Gillespie, J. Price-O'Brien, A. C. Loos, *Compos. Sci. Technol.* **2006**, *66*, 102; b) R. Kozlowski, B. Mieleniak, M. Muzyczek, A. Kubacki, *Fire Mater.* **2002**, *26*, 243.

[11] a) A. Agarwal, A. Raheja, T. S. Natarajan, T. S. Chandra, *Innovative Food Sci. Emerging Technol.* **2014**, *26*, 424; b) M. M. Bergshoef, G. J. Vancso, *Adv. Mater.* **1999**, *11*, 1362; c) S. K. Bhullar, B. Kaya, M. B. G. Jun, *J. Polym. Environ.* **2015**, *23*, 416; d) W. Chalco-Sandoval, M. J. Fabra, A. Lopez-Rubio, J. M. Lagaron, *J. Appl. Polym. Sci.* n/a, **2014**, *131*.

[12] J. C. Park, *Republic of Korea Patent KR100787624B1*, **2007**.

[13] a) E. S. Medeiros, G. M. Glenn, A. P. Klamczynski, W. J. Orts, L. H. C. Mattoso, *J. Appl. Polym. Sci.* **2009**, *113*, 2322; b) J. E. Oliveira, L. H. C. Mattoso, W. J. Orts, E. S. Medeiros, *Adv. Mater. Sci. Eng.* **2013**, *2013*, 14.

[14] J. E. Oliveira, E. A. Moraes, R. G. F. Costa, A. S. Afonso, L. H. C. Mattoso, W. J. Orts, E. S. Medeiros, *J. Appl. Polym. Sci.* **2011**, *122*, 3396.

[15] S. H. Park, S. M. Lee, H. S. Lim, J. T. Han, D. R. Lee, H. S. Shin, Y. J. Jeong, J. Kim, J. H. Cho, *ACS Appl. Mater. Interfaces* **2010**, *2*, 658.

[16] Y. M. Chi, T. P. Jung, G. Cauwenberghs, *IEEE Rev. Biomed. Eng.* **2010**, *3*, 106.

[17] P. R. Cavanagh, P. V. Komi, *Eur. J. App. Physiol. Occup. Physiol.* **1979**, *42*, 159.

[18] W. Boucsein, D. C. Fowles, S. Grimnes, G. Ben-Shakhar, W. T. Roth, M. E. Dawson, D. L. Filion, S. P. R. A. Hoc, *Psychophysiology* **2012**, *49*, 1017.

[19] R. Zangroniz, A. Martinez-Rodrigo, J. M. Pastor, M. T. Lopez, A. Fernandez-Caballero, *Sensors* **2017**, *17*, 2324.

[20] N. H. Liu, C. Y. Chiang, H. C. Chu, *Sensors* **2013**, *13*, 10273.